Letter

Observing the ping-pong modality of the isospin degree of freedom in cluster emission from heavy-ion reactions

Yijie Wang,[1,*] Fenhai Guan,[1] Xinyue Diao,[1] Mengting Wan,[2,3] Yuhao Qin,[1] Zhi Qin,[1] Qianghua Wu,[1] Dong Guo,[1] Dawei Si,[1] Sheng Xiao,[1] Boyuan Zhang,[1] Yaopeng Zhang,[1] Baiting Tian,[4] Xianglun Wei,[5] Herun Yang,[5] Peng Ma,[5] Rongjiang Hu,[5] Limin Duan,[5] Fangfang Duan,[5] Qiang Hu,[5] Junbing Ma,[5] Shiwei Xu,[5] Zhen Bai,[5] Yanyun Yang,[5] Jiansong Wang,[5,6] Wenbo Liu,[7] Wanqing Su,[7] Xiaobao Wei,[7] Chun-Wang Ma,[7] Xinxiang Li,[8,9] Hongwei Wang,[9,10] Fangyuan Wang,[11] Yingxun Zhang,[11] Michał Warda,[12] Arthur Dobrowolski,[12] Bożena Nerlo-Pomorska,[12] Krzysztof Pomorski,[12] Li Ou,[2,3,†] and Zhigang Xiao[1,13,‡]

[1]*Department of Physics, Tsinghua University, Beijing 100084, China*
[2]*College of Physics and Technology, Guangxi Normal University, Guilin 541004, China*
[3]*Guangxi Key Laboratory of Nuclear Physics and Technology, Guangxi Normal University, Guilin 541004, China*
[4]*College of Physics, Sichuan University, Sichuan, 610065, China*
[5]*Institute of Modern Physics, Chinese Academy of Sciences, Lanzhou 730000, China*
[6]*School of Science, Huzhou University, Huzhou, 313000, China*
[7]*Institute of Particle and Nuclear Physics, Henan Normal University, Xinxiang 453007, China*
[8]*School of Nuclear Science and Technology, University of South China, Hengyang 421001, China*
[9]*Shanghai Institute of Applied Physics, Chinese Academy of Science, Shanghai 201800, China*
[10]*Shanghai Advanced Research Institute, Chinese Academy of Science, Shanghai 201210, China*
[11]*China Institute of Atomic Energy, Beijing 102413, China*
[12]*Institute of Physics, Maria Curie Skłodowska University, 20-031 Lublin, Poland*
[13]*Collaborative Innovation Center of Quantum Matter, Tsinghua University, Beijing 100084, China*

(Received 12 September 2022; revised 20 February 2023; accepted 31 March 2023; published 11 April 2023)

Thermodynamic and chemical two-body correlations of the isotope-resolved clusters are measured in $^{86}\mathrm{Kr}+{}^{208}\mathrm{Pb}$ reactions at 25 MeV/u. The yield and kinetic variables of the $A=3$ isobars are analyzed in coincidence with the intermediate mass fragments of $6 \leqslant A \leqslant 11$. While the velocity spectra of both t and ^{3}He exhibit scaling behavior over the type of the intermediate mass fragments, the yield ratios of $t/{}^3$He correlate reversely to the neutron-to-proton ratio N/Z of the latter, showing the ping-pong modality of the N/Z of the emitted particles. The commonality that the N/Z of the residues keeps the initial system value is extended to the cluster emission in heavy ion reactions. The comparison to transport model calculations to the data is discussed.

DOI: 10.1103/PhysRevC.107.L041601

Introduction. Heavy ion reaction (HIR) is a femtoscopic nonequilibrium process, where neutrons and protons transport differently [1]. Relying on transport model description on a variety of observables in HIRs, one can unveil the equation of state of nuclear matter (nEOS), which is essential to describe the explosive events of dense stellar objects where the heavy elements are created in the universe [2–5]. The large uncertainties of the nEOS come from its isospin vector part, namely the density dependent nuclear symmetry energy $E_{\mathrm{sym}}(\rho)$ [6], a longstanding frontier bridging astrophysics and nuclear physics. The accurate constraint of $E_{\mathrm{sym}}(\rho)$ becomes more indispensable than ever since the detection of the gravitational wave from GW170817 [7–9].

Despite large progress on constraining $E_{\mathrm{sym}}(\rho)$ in terrestrial nuclear laboratories [10–19], the slope parameter of $E_{\mathrm{sym}}(\rho)$ suffers 30% uncertainty and the symmetry energy at about $2\rho_0$ is even less constrained. To achieve accurate results, great efforts are demanded to improve the reliability of the theoretical models [20–24] and to accumulate more experimental data containing isospin sensitive probes [25,26].

The ongoing endeavors encounter unavoidably two fundamental questions arising from the thermodynamic and chemical complication of HIRs. One is the transport of a given degree of freedom (DOF) in a dynamic process, i.e., how does the DOF of isospin (IDOF) evolve in HIRs? The question stimulates enormous progress on isospin chronology applications [27–32]. The other is clustering, which makes it more complicated to probe $E_{\mathrm{sym}}(\rho)$ using HIRs, since cluster formation influences the isospin transport and the yield of the final products [33].

To this end, it is essential to elucidate the two questions and their interplay in the specific HIRs before the $E_{\mathrm{sym}}(\rho)$ can be stringently constrained. We are motivated to illustrate how the IDOF evolves with the presence of cluster emission in HIRs by introducing the temporal two-body correlation analysis.

*yj-wang15@tsinghua.org.cn
†liou@gxnu.edu.cn
‡xiaozg@tsinghua.edu.cn

The motivation is novel, because the isospin observables from HIRs are so far mostly one-body quantity, which prevents to draw detailed and comprehensive picture on how the IDOF evolves with the presence of clustering. Among many existed observables, the ratio of $A = 3$ isobars, $t/^3$He, has been identified to probe $E_{\rm sym}(\rho)$ both theoretically [17,18,34–40] and experimentally [40–48].

In this letter, the thermodynamic and chemical correlations of the $A = 3$ isobars and the intermediate mass fragments (IMFs) are analyzed in 25 MeV/u ^{86}Kr + ^{208}Pb reactions. The anticorrelation of the ratio $t/^3$He with the N/Z of the heavy fragments are observed, showing a novel ping-pong modality. Further, we report the commonality that the N/Z of the initial system undergoing cluster emission is kept in various nuclear processes. The comparison of the data to the transport model simulations is discussed.

Experimental setup. The experiment was performed with the Compact Spectrometer for Heavy IoN Experiment (CSHINE) [49,50], installed at the final focal plane of the Radioactive Ion Beam Line at Lanzhou (RIBLL-I) [51]. The 25 MeV/u ^{86}Kr beam was delivered by the Heavy Ion Research Facility at Lanzhou (HIRFL) [52], bombarding a natural lead target with the thickness of 1 mg/cm^2. In the current configuration of CSHINE, light charged particles (LCPs) and IMFs are measured by four silicon-strip detector telescopes (SSDTs), while the coincident fission fragments (FFs) are measured by three parallel plate avalanche counters (PPACs), each covering a sensitive area of 240×280 mm^2. Each SSDT consists of one single-sided silicon-strip detector (SSSSD) and one double-sided silicon strip detector (DSSSD), backed by a 3×3 CsI(Tl) crystal hodoscope with length of 50 mm. The sensitive area of each SSDT is 64×64mm^2, and the granularity is 4×4 mm^2 delivering about 1° angular resolution. The SSDTs cover the angular range of 10°–60° in laboratory. The energy resolution of the SSDT is better than 2%, and the isotopes up to $Z = 6$ can be identified. For the technical details of the CSHINE, one can refer to [49,50]. Since the event statistics of the four-body coincidence, i.e., with two charged particles in SSDTs and two FFs in PPACs, does not suffice, here, we analyze the two-body coincidence of two fragments in the SSDTs. Multihits and signal sharing are treated with care in the track recognition, the overall track recognition efficiency is about 90%. The detailed procedure of track reconstruction can be found in [53].

Figure 1 summarizes the data used in the current analysis. Panel (a) presents the scatter plot of $\Delta E_2 - E_{\rm CsI}$ of the SSDT1. It is shown that all the isotopes can be identified clearly to $Z = 6$. Panel (b) presents the PID plots for all isotopes on $\Delta E_2 - E_{\rm CsI}$ summed over SSDT 1 to 4 after the tracking procedure [53]. Panels (c) and (d) present scatter plots of longitudinal vs. transverse velocity distributions of triton and ^{3}He stopped in the CsI(Tl) hodoscope, respectively.

Results and Discussions. In order to observe the temporally correlated emissions of charged particles, we investigate the two-body events in the SSDTs, with one being the LCP, $F_L(Z_L, A_L)$, the other being a IMF, $F_H(Z_H, A_H)$, with $6 \leqslant A_H \leqslant 11$, where the subscripts L and H denote *light* and *heavy* to differentiate the two particles, respectively. Here, F_L is chosen as one of the mirror nuclei, triton, or ^{3}He. According to earlier studies using correlation function method, the heavy fragments are emitted with an averagely shorter time constant at this energy region [54]. Thus, it is reasonable to assume that the F_H is emitted earlier than F_L in our study. To circumvent the spectrum discontinuity caused by the gap between ΔE_1 and ΔE_2, only the particles F_L stopped in the CsI(Tl) hodoscope are analyzed.

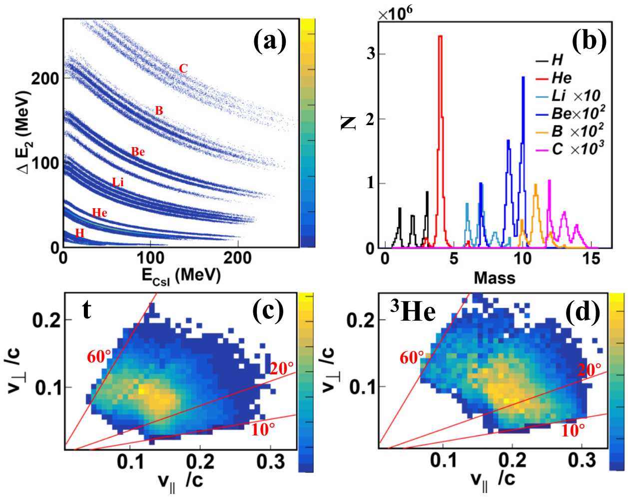

FIG. 1. The scatter plot of $\Delta E_2 - E_{\rm CsI}$ of the SSDT1 (a). The PID plots for all isotopes on $\Delta E_2 - E_{\rm CsI}$ summed over SSDT 1 to 4 (b). The scatter plots of longitudinal vs. transverse velocity distributions of triton and ^{3}He are plotted in (c) and (d), respectively. The azimuthal efficiency is corrected.

We first check the thermodynamic correlation of F_L and F_H. Figures 2(a) and 2(b) present the velocity spectra of triton (a) and ^{3}He (b) in coincidence with various IMFs F_H. It is shown that the shape and the range of the velocity distributions of triton and ^{3}He exhibit insignificant dependence on the type of F_H, although the coincident yield differs. Normalizing the yields to the histograms in the case where F_H is ^{7}Li, one

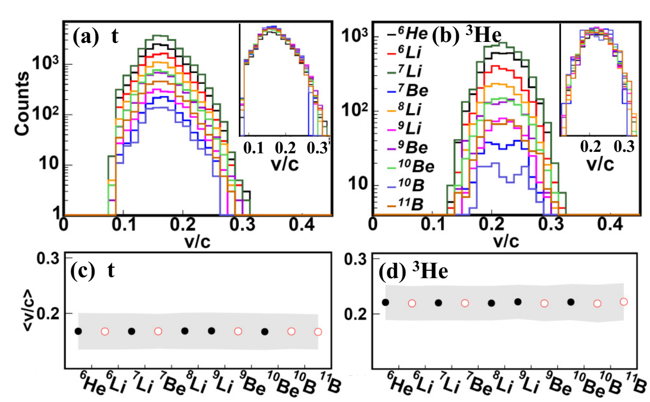

FIG. 2. The spectra of the velocities (in unit of c) of triton (a) and ^{3}He (b) in coincidence with various F_H of $A_H = 6$ to 11. The lower panels present the mean velocity $\langle v\rangle$ of t (c) and ^{3}He (d), with the solid (open) circles denoting the coincident F_H of larger (smaller) neutron richness, respectively. The shadowing band denotes the standard deviation of each corresponding spectrum.

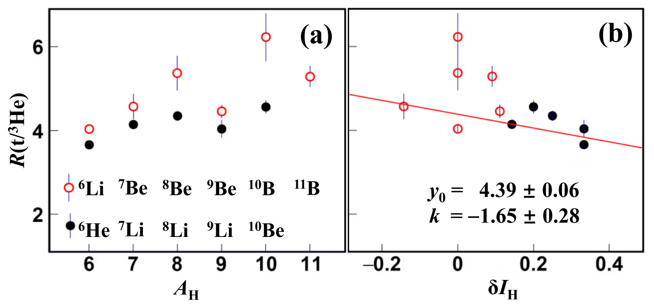

FIG. 3. (a) Yield ratio of $R(t/^3\mathrm{He})$ in coincidence with different IMFs, the solid (open) circles represent the IMF of larger (smaller) neutron richness at a given mass number. (b) $R(t/^3\mathrm{He})$ as a function of the neutron richness δI_{H} of F_{H}. k and y_0 are the slope and the intercept parameters of the linear fit, respectively. The error bars are of only statistical origin.

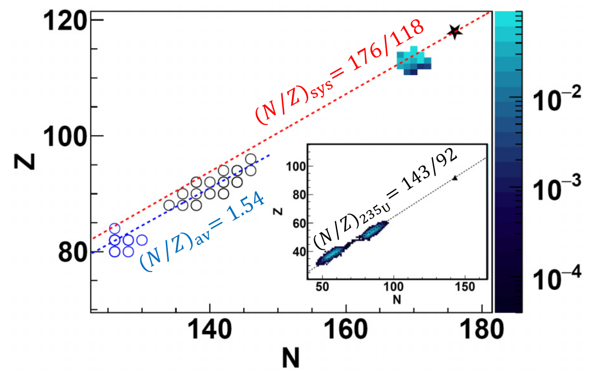

FIG. 4. The correlation between the N/Z of the initial system and the remaining nuclei. The asterisk denotes the initial $^{86}\mathrm{Kr} + {}^{208}\mathrm{Pb}$ system, and the colored contour represents the probability distribution of the remaining nuclei after the emission of $\mathrm{F_H}$ and $\mathrm{F_L}$. The circles denote the cluster decay of various superheavy nuclei, with the black (blue) ones being the parents (daughters). The inset displays the yield distribution of the n-induced fission of $^{235}\mathrm{U}$ on the $N-Z$ plot.

sees that all the spectra exhibit scaling behavior, as shown in the insets in (a) and (b). Furthermore, the mean velocity $\langle v \rangle$ of triton and ^{3}He are presented in (c) and (d), varying with the type of $\mathrm{F_H}$. The shadowing band represents the standard deviation σ_v of each individual v spectrum. The solid (open) symbols denote the $\mathrm{F_H}$ with larger (smaller) neutron richness, respectively. Clearly, both $\langle v \rangle$ and σ_v are nearly constant, showing insignificant dependence on the N/Z of $\mathrm{F_H}$. It suggests that the two $A = 3$ isobars experience the same dynamic process, regardless of whether the correlated IMFs are rich or deficient in neutrons.

Surprisingly, however, the IDOF features differently. Figure 3(a) presents the yield ratio of $t/^3\mathrm{He}$, written as $R(t/^3\mathrm{He})$, as a function of A_{H}. Again, the solid (open) symbols correspond to the more (less) neutron-rich $\mathrm{F_H}$ at a given mass (here, neutron-rich only has its relative meaning in the $\mathrm{F_H}$ pair with the same mass). The IMF ^{8}Be is reconstructed by two correlated α particles. It is seen that the ratio $R(t/^3\mathrm{He})$ splits in two groups. A ping-pong motion modality of the N/Z in cluster emission is suggested: after a neutron-rich IMF (solid) is emitted, the $R(t/^3\mathrm{He})$ is smaller, indicating that a less neutron-rich $\mathrm{F_L}$ follows. Oppositely, if the $\mathrm{F_H}$ is less neutron rich (open), $R(t/^3\mathrm{He})$ is larger, indicating that $\mathrm{F_L}$ is averagely more neutron-rich. The ping-pong behavior of the N/Z of the two clusters demonstrates that the isospin content of $\mathrm{F_L}$ depends on the N/Z of $\mathrm{F_H}$ emitted at earlier chance. This tendency is further presented in panel (b), where the $R(t/^3\mathrm{He})$ is plotted as a function of the relative neutron richness of $\mathrm{F_H}$ defined by $\delta I_{\mathrm{H}} = (N_{\mathrm{H}} - Z_{\mathrm{H}})/A_{\mathrm{H}}$. The solid line is the least square linear fit to the data points. A nonzero minus slope k is convinced at 5.8σ confidential level, evidencing that the isospin compositions of $\mathrm{F_H}$ and $\mathrm{F_L}$ are anticorrelated.

Model independently, the anticorrelation between the N/Z of $\mathrm{F_L}$ and $\mathrm{F_H}$ infers how the IDOF evolves during the decay of the highly excited system formed in HIRs. If more (less) neutrons are carried away by the IMF, the following LCP carries less (more) neutrons, as a consequence of neutron and proton (isospin) conservation in the reaction system of finite size. It suggests that for the decay of such a finite size system, the neutron richness of the emitted particles is balanced near a certain value, so that the remaining system, possibly destined to emission residue or fission, possesses a certain N/Z close to that of the initial system, see below.

In order to show the isospin balancing effect clearly, Fig. 4 presents the $N-Z$ correlation of the remaining nuclei, obtained by subtracting $\mathrm{F_L}$ and $\mathrm{F_H}$ from the initial system. The $N/Z = 176/118$ relationship is indicated by the red dashed line, and the asterisk denotes the location of the $^{86}\mathrm{Kr} + {}^{208}\mathrm{Pb}$ system. It is shown that the remaining system situates in the vicinity of the dashed line, indicating that the average N/Z of the remaining system is the same as the initial value of $^{86}\mathrm{Kr} + {}^{208}\mathrm{Pb}$. Here, we can only count the two clusters measured, including $A = 3$ isobars and the IMFs. Because of the anticorrelation demonstrated in Fig. 3, it is reasonable to assume the undetected decay particles have a similar N/Z to the detected products and hence do not drag the distribution center away from the dashed line.

Interestingly, the cluster radioactivity observed in various superheavy nuclei [55–57] is similar, as shown by the circles in the plot. The cluster decay channels are taken from [56]. It is seen that the daughters (blue) are distributed near the same N/Z line of the parent nuclei (black). Moreover, if one inspects the fission of heavy nuclei, for instance, the neutron induced fission of ^{235}U plotted in the inset, the N/Z of the fission fragments follows the same N/Z value of the parent nucleus ^{235}U [58]. Because of the presence of $E_{\mathrm{sym}}(\rho)$, which finally goes into the Q value, the N/Z of the daughters inherits that of the parents. This is commonly observed in fission and in the cluster decay of heavy nuclei. Our experiment extends the commonality to the cluster emission of the finite and highly excited system formed in HIRs. The commonality also supports that the $E_{\mathrm{sym}}(\rho)$ is at work in the anticorrelation of the N/Z of $\mathrm{F_L}$ and $\mathrm{F_H}$ emission, in addition to the neutron and proton number conservation.

Comparison to transport model simulations. To understand the isospin transport behavior, the reaction process is simu-

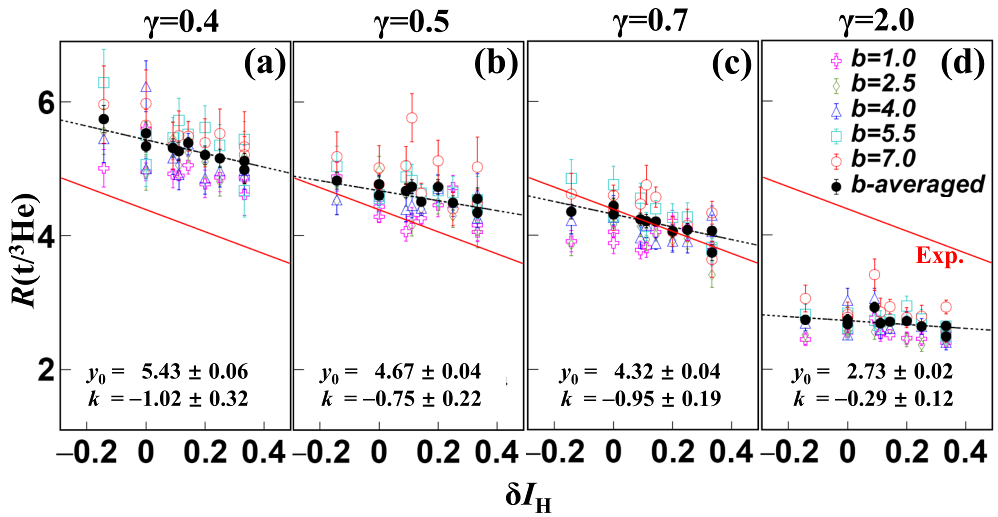

FIG. 5. Yield ratio of $R(t/{}^3\mathrm{He})$ by ImQMD simulations as a function of δI_{H} with $\gamma = 0.4$, 0.5, 0.7, and 2.0, respectively. The results with $b = 1$ to 7 fm are represented by the open symbols, on top of which the b-averaged results are presented by the solid circles with the linear fit (dashed line).

lated using the improved quantum molecular dynamics model (ImQMD05) [59] followed by a statistic decay afterburner GEMINI [60,61]. The ImQMD05 model [59] was developed from the original version of the quantum molecular dynamics code proposed by Aichelin *et al.* [62,63], and has been a useful tool to explore the reaction dynamics of HICs in low and intermediate energies for understanding the nuclear phenomena. For brevity, we limit our discussion here to the mean field part of the ImQMD05 model, where the symmetry potential energy is involved. The local nuclear potential energy density functional in the ImQMD05 model is written as

$$V_{\mathrm{loc}} = \frac{\alpha}{2}\frac{\rho^2}{\rho_0} + \frac{\beta}{\eta+1}\frac{\rho^{\eta+1}}{\rho_0^{\eta}} + \frac{g_{\mathrm{sur}}}{2\rho_0}(\nabla\rho)^2 + \frac{g_{\mathrm{sur,iso}}}{\rho_0}[\nabla(\rho_{\mathrm{n}}-\rho_{\mathrm{p}})]^2 + g_{\rho\tau}\frac{\rho^{8/3}}{\rho_0^{5/3}} + \frac{C_{\mathrm{s}}}{2}\frac{\rho^{\gamma+1}}{\rho_0^{\gamma}}\delta^2, \tag{1}$$

where ρ, ρ_{n}, ρ_{p} are the nucleon, neutron, and proton density, respectively. $\delta = (\rho_{\mathrm{n}} - \rho_{\mathrm{p}})/(\rho_{\mathrm{n}} + \rho_{\mathrm{p}})$ is the isospin asymmetry degree. In this work, the parameters in Eq. (1) are determined by the MSL0 parameter set [64], in which the parameter γ is adjusted to mimicked the various density behavior of symmetry potential energy. The simulations cover the impact parameter range of $1.0 \leqslant b \leqslant 11.5$ fm with steps of $\Delta b = 1.5$ fm. For each b, 5×10^5 events were simulated. At the end of the ImQMD calculations, clusters are recognized by a minimum spanning tree (MST) algorithm [63,65] widely used in the quantum molecular dynamics calculations. The information of the excited cluster is input into the GEMINI model to perform statistical decay calculations. The same velocity and polar angle cuts are adopted to t and ^{3}He as in experiment. To avoid the ambiguity of the correlation, we exclude the events containing more than one $\mathrm{F_H}$ with the same N_{H} and A_{H}, but set no cut on the multiplicity of F_{L}.

Figure 5 presents the $R(t/{}^3\mathrm{He})$ ratio as a function of δI_{H} for different $E_{\mathrm{sym}}(\rho)$ with $\gamma = 0.4$, 0.5, 0.7, and 2.0, respectively. The value of $R(t/{}^3\mathrm{He})$ depends sensitively on $E_{\mathrm{sym}}(\rho)$, consistent with [34], but less sensitive on b, as shown by the open symbols in panels (a)–(d). The b-weighted average ratios are depicted by the solid circles with linear fit (dashed line). The experimental trend is replotted in solid lines for comparison. Interestingly, the anticorrelation trend between $R(t/{}^3\mathrm{He})$ and δI_{H} is qualitatively reproduced, but the slope is generally underestimated in the simulation. The superstiff ($\gamma = 2.0$) and the supersoft ($\gamma = 0.4$) parametrizations of $E_{\mathrm{sym}}(\rho)$ are disfavored by the large deviation from the experimental trend. By varying γ from 0.5 to 0.7, the simulations cross over the experimental area.

The comparison has an important implication. If one only looks at the integrated $R(t/{}^3\mathrm{He})$, i.e., the projection of the data points to the ordinate, apparently $\gamma = 0.7$ is favored, as shown in Fig. 5(c). Nevertheless, the distribution of integrated $R(t/{}^3\mathrm{He})$ is broadened since its average value varies with the N/Z of the coincident IMF, even with a well-determined impact parameter. In other words, the measurement of the anticorrelation between $R(t/{}^3\mathrm{He})$ and δI_{H} provides an extra dimension to reveal finely the isospin dynamics in presence of clustering in the finite system, which is hardly realizable through the integrated $R(t/{}^3\mathrm{He})$ as a one-body quantity. Since the discrepancy on the slope is still evident between the data and the simulations, we do not quantify $E_{\mathrm{sym}}(\rho)$ more precisely here. Instead, with this new line, we suggest that the modeling of clustering in HIRs with transport theory requires further efforts, even for the $A = 3$ clusters, of which the origin is very complicated.

It is important to ensure that the experimental coverage is mainly contributed by the intermediate velocity source. From the velocity distribution shown in Fig. 1(c) and 1(d), one sees no separated contribution from the projectile-like fragment (PLF) source, which is characterized by small transverse velocity and longitudinal one close to that of projectile. To be more convincing, the velocity distribution of ImQMD calculations is studied. Figure 6 presents the scatter plots of

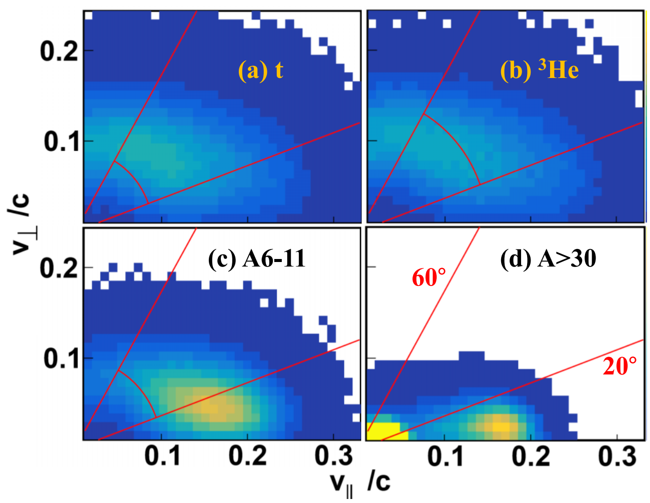

FIG. 6. The scatter plots of longitudinal vs. transverse velocity distributions in ImQMD simulation for triton (a), ^{3}He (b), IMFs with $6 \leqslant A \leqslant 11$ (c), and heavy residues with $A > 30$ (d). The experimental angular and velocity cuts are presented in (a) to (c).

longitudinal vs. transverse velocity distributions for the products with different masses in ImQMD simulations. Unlike the heavy residues of $A > 30$ shown in (d), where both components of the PLF and the target-like fragment (TLF) are clearly seen, the LCPs with $A = 3$ do not exhibit obvious contribution from PLF in the angular range of our study, as shown in panels (a) and (b). With increasing the mass, the distribution becomes more forward peaked but is still far from the location of PLF with $A > 30$, as shown in panel (c) for F_H under investigation. In our analysis, in order to suppress maximally the contribution from the PLF source, we adjusted the lower angular cut from 10° to 20°. When the cut is loosened to 10° and F_H with $A \leqslant 14$ can be included, the ping-pong modality remains robustly clear and the conclusion is not changed.

Experimentally, it is also important to select the certain centrality of the reaction. As presented in Fig. 5, a selection of the impact parameter increases the precision of constraining $E_{sym}(\rho)$. But this is not done due to the lower statistics of four-body events. Nevertheless, because our SSDTs covers only part of a solid angle, it is less likely that two or more LCPs and IMFs can be recorded by the SSDT array in a very peripheral reactions. It is presumable that two-body correlation in the SSDTs has some selection ability to the impact parameter, particularly one fragment is in an intermediate mass range. Again, one can check this presumption using transport model simulations by counting the correlations of F_L and F_H out of the total events. Defining the total weight of the pair correlation by

$$W_{LH} = b \cdot n_{LH}(b)/N_{tot}(b), \tag{2}$$

where n_{LH} are the number of the correlated pairs of F_L and F_H counted in N_{tot} events simulated at a given impact parameter b. The velocity and polar angle cuts are taken as the same as in experiment. As plotted in Fig. 7, the weight starts at a very low level at central collisions and reaches the top at semicentral ones before decreasing rapidly at large b, suggesting that the correlation observable selects mainly the semicentral collisions. It supports the effectiveness of the range of $1.0 < b < 11.5$ fm taken in the simulations for the comparison presented in Fig. 5.

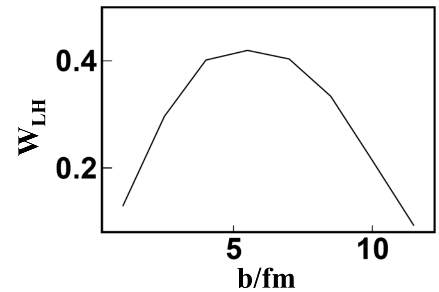

FIG. 7. The weight of the events containing F_L and F_H correlation as a function of impact parameter b in ImQMD simulations with $\gamma = 0.5$.

Conclusion. Transport of isospin degree of freedom and cluster formation are two extremely important aspects of HIRs. To understand the two aspects, the $A = 3$ isobars are analyzed in coincidence with fragments of $6 \leqslant A \leqslant 11$ in 25 MeV/u ^{86}Kr + ^{208}Pb reactions. While the velocity spectra of triton and ^{3}He show scaling behavior over the type of the intermediate mass fragments, the yield ratio $R(t/^3\text{He})$ exhibits evident anticorrelation with the N/Z of the latter, suggesting the ping-pong modality of the N/Z of the emitted particles. The commonality that the remaining system inherits the N/Z of the initial system, which has been reported in cluster decay and fission of superheavy nuclei, is extended to the cluster emission from HIRs in Fermi energy region. In addition to the yield ratio of $t/^3$He, the anticorrelation between the N/Z of the two clusters, being sensitive to the isospin dynamics in a finite-size system, provides a benchmark to test the transport theory in terms of cluster formation and isospin dynamics, and helps eventually achieving stringent constraint of $E_{sym}(\rho)$ near the saturation density using heavy ion reactions.

*Acknowledgments.*This work is supported by the Ministry of Science and Technology under Grants No. 2022YFE0103400 and No. 2020YFE0202001, and by the National Natural Science Foundation of China under Grants No. 11961131010, No. 11961141004, No. 12205160, and No. 11965004, and by the Polish National Science Center under Grant No. 2018/30/Q/ST2/00185. Z.G.X. is also supported by Tsinghua University Initiative Scientific Research Program and the Heavy Ion Research Facility at Lanzhou (HIRFL). The authors thank Prof. Pengfei Zhuang from THU, Yueheng Lan from BUPT and Prof. Nobuaki Imai from University of Tokyo for their valuable discussions.

[1] M. Colonna, Collision dynamics at medium and relativistic energies, Prog. Part. Nucl. Phys. **113**, 103775 (2020).
[2] B.-A. Li, B.-J. Cai, W.-J. Xie, and N.-B. Zhang, Progress in constraining nuclear symmetry energy using neutron

star observables since GW170817, Universe **7**, 182 (2021).
[3] S. Huth *et al.*, Constraining neutron-star matter with microscopic and macroscopic collisions, Nature (London) **606**, 276 (2022).
[4] A. W. Steiner, M. Prakash, J. M. Lattimer, and P. J. Ellis, Isospin asymmetry in nuclei and neutron stars, Phys. Rep. **411**, 325 (2005).
[5] M. Oertel, M. Hempel, T. Klähn, and S. Typel, Equations of state for supernovae and compact stars, Rev. Mod. Phys. **89**, 015007 (2017).
[6] B.-A. Li, L.-W. Chen, and C. M. Ko, Recent progress and new challenges in isospin physics with heavy-ion reactions, Phys. Rep. **464**, 113 (2008).
[7] B. P. Abbott *et al.*, GW170817: Observation of Gravitational Waves from a Binary Neutron Star Inspiral, Phys. Rev. Lett. **119**, 161101 (2017).
[8] B. P. Abbott *et al.*, GW170817: Measurements of Neutron Star Radii and Equation of State, Phys. Rev. Lett. **121**, 161101 (2018).
[9] S. De, D. Finstad, J. M. Lattimer, D. A. Brown, E. Berger, and C. M. Biwer, Tidal Deformabilities and Radii of Neutron Stars from the Observation of GW170817, Phys. Rev. Lett. **121**, 091102 (2018); **121**, 259902(E) (2018).
[10] B.-A. Li, C. M. Ko, and Z.-z. Ren, Equation of State of Asymmetric Nuclear Matter and Collisions of Neutron-Rich Nuclei, Phys. Rev. Lett. **78**, 1644 (1997).
[11] Y.-x. Zhang and Z.-x. Li, Probing the density dependence of the symmetry potential with peripheral heavy-ion collisions, Phys. Rev. C **71**, 024604 (2005).
[12] B.-A. Li, Probing the High Density Behavior of the Nuclear Symmetry Energy with High Energy Heavy-Ion Collisions, Phys. Rev. Lett. **88**, 192701 (2002).
[13] Z. Xiao, B.-A. Li, L.-W. Chen, G.-C. Yong, and M. Zhang, Circumstantial Evidence for a Soft Nuclear Symmetry Energy at Suprasaturation Densities, Phys. Rev. Lett. **102**, 062502 (2009).
[14] J. Estee *et al.*, Probing the Symmetry Energy with the Spectral Pion Ratio, Phys. Rev. Lett. **126**, 162701 (2021).
[15] G. Ferini, T. Gaitanos, M. Colonna, M. Di Toro, and H. H. Wolter, Isospin Effects on Subthreshold Kaon Production at Intermediate Energies, Phys. Rev. Lett. **97**, 202301 (2006).
[16] G.-C. Yong, B.-A. Li, Z.-G. Xiao, and Z.-W. Lin, Probing high-density nuclear symmetry energy with Ξ^-/Ξ^0 ratio in heavy-ion collisions at $\sqrt{s_{NN}} \sim 3$ GeV, Phys. Rev. C **106**, 024902 (2022).
[17] L.-W. Chen, C. M. Ko, and B.-A. Li, Light clusters production as a probe to the nuclear symmetry energy, Phys. Rev. C **68**, 017601 (2003).
[18] Q. Li, Z. Li, S. Soff, M. Bleicher, and H. Stoecker, Probing the density dependence of the symmetry potential at low and high densities, Phys. Rev. C **72**, 034613 (2005).
[19] B.-A. Li, A. Ramos, G. Verde, and I. Vidana, Topical issue on nuclear symmetry energy, Eur. Phys. J. A **50**, 9 (2014).
[20] J. Xu, Transport approaches for the description of intermediate-energy heavy-ion collisions, Prog. Part. Nucl. Phys. **106**, 312 (2019).
[21] Y.-J. Wang and Q.-F. Li, Application of microscopic transport model in the study of nuclear equation of state from heavy ion collisions at intermediate energies, Front. Phys. (Beijing) **15**, 44302 (2020).
[22] Y.-X. Zhang *et al.*, Comparison of heavy-ion transport simulations: Collision integral in a box, Phys. Rev. C **97**, 034625 (2018).
[23] A. Ono *et al.*, Comparison of heavy-ion transport simulations: Collision integral with pions and Δ resonances in a box, Phys. Rev. C **100**, 044617 (2019).
[24] M. Colonna *et al.*, Comparison of heavy-ion transport simulations: Mean-field dynamics in a box, Phys. Rev. C **104**, 024603 (2021).
[25] Y. Zhang, J. Tian, W. Cheng, F. Guan, Y. Huang, H. Li, L. Lu, R. Wang, Y. Wang, Q. Wu, H. Yi, Z. Zhang, Y. Zhao, L. Duan, R. Hu, M. Huang, G. Jin, S. Jin, C. Lu, J. Ma *et al.*, Long-time drift of the isospin degree of freedom in heavy ion collisions, Phys. Rev. C **95**, 041602(R) (2017).
[26] L. Ou, Z. Xiao, H. Yi, N. Wang, M. Liu, and J. Tian, Dynamic Isovector Reorientation of Deuteron as a Probe to Nuclear Symmetry Energy, Phys. Rev. Lett. **115**, 212501 (2015).
[27] A. Jedele *et al.*, Characterizing Neutron-Proton Equilibration in Nuclear Reactions with Subzeptosecond Resolution, Phys. Rev. Lett. **118**, 062501 (2017).
[28] A. Rodriguez Manso, A. B. McIntosh, A. Jedele, K. Hagel, L. Heilborn, Z. Kohley, L. W. May, A. Zarrella, and S. J. Yennello, Detailed characterization of neutron-proton equilibration in dynamically deformed nuclear systems, Phys. Rev. C **95**, 044604 (2017).
[29] Y. Wang *et al.*, The emission order of hydrogen isotopes via correlation functions in 30 MeV/u Ar+Au reactions, Phys. Lett. B **825**, 136856 (2022).
[30] R. Ghetti *et al.*, Chronology of Particle Emission from the E/A= 61 MeV ^{36}Ar + ^{27}Al Reaction, Phys. Rev. Lett. **91**, 092701 (2003).
[31] R. Ghetti, V. Avdeichikov, B. Jakobsson, P. Golubev, J. Helgesson, N. Colonna, G. Tagliente, H. W. Wilschut, S. Kopecky, V. L. Kravchuk, E. W. Anderson, P. Nadel-Turonski, L. Westerberg, V. Bellini, M. L. Sperduto, and C. Sutera, Isospin effects on two particle correlation functions in E/A = 61-MeV Ar-36 + Sn-112, Sn-124 reactions, Phys. Rev. C **69**, 031605(R) (2004).
[32] G. Verde, A. Chbihi, R. Ghetti, and J. Helgesson, Correlations and characterization of emitting sources, Eur. Phys. J. A **30**, 81 (2006).
[33] A. Ono, Dynamics of clusters and fragments in heavy-ion collisions, Prog. Part. Nucl. Phys. **105**, 139 (2019).
[34] L.-W. Chen, C. M. Ko, and B.-A. Li, Light cluster production in intermediate-energy heavy ion collisions induced by neutron rich nuclei, Nucl. Phys. A **729**, 809 (2003).
[35] Y. Wang, C. Guo, Q. Li, and H. Zhang, ^{3}H / ^{3}He ratio as a probe of the nuclear symmetry energy at sub-saturation densities, Eur. Phys. J. A **51**, 37 (2015).
[36] T. Gaitanos, M. Colonna, M. Di Toro, and H. H. Wolter, Stopping and isospin equilibration in heavy ion collisions, Phys. Lett. B **595**, 209 (2004).
[37] G.-C. Yong, B.-A. Li, L.-W. Chen, and X.-C. Zhang, Triton-He-3 relative and differential flows as probes of the nuclear symmetry energy at supra-saturation densities, Phys. Rev. C **80**, 044608 (2009).
[38] P. Chomaz and F. Gulminelli, Phase transition in an isospin dependent lattice gas model, Phys. Lett. B **447**, 221 (1999).
[39] S. Albergo, S. Costa, E. Costanzo, and A. Rubbino, Temperature and free-nucleon densities of nuclear matter exploding into

light clusters in heavy-ion collisions, Nuovo Cimento A **89**, 1 (1985).

[40] J. F. Dempsey *et al.*, Isospin dependence of intermediate mass fragment production in heavy-ion collisions at E/A=55 MeV, Phys. Rev. C **54**, 1710 (1996).

[41] W. Reisdorf *et al.*, Systematics of central heavy ion collisions in the 1A GeV regime, Nucl. Phys. A **848**, 366 (2010).

[42] H. S. Xu *et al.*, Isospin Fractionation in Nuclear Multifragmentation, Phys. Rev. Lett. **85**, 716 (2000).

[43] M. A. Famiano, T. Liu, W. G. Lynch, A. M. Rogers, M. B. Tsang, M. S. Wallace, R. J. Charity, S. Komarov, D. G. Sarantites, and L. G. Sobotka, Neutron and Proton Transverse Emission Ratio Measurements and the Density Dependence of the Asymmetry Term of the Nuclear Equation of State, Phys. Rev. Lett. **97**, 052701 (2006).

[44] S. Nagamiya, M. C. Lemaire, E. Moller, S. Schnetzer, G. Shapiro, H. Steiner, and I. Tanihata, Production of pions and light fragments at large angles in high-energy nuclear collisions, Phys. Rev. C **24**, 971 (1981).

[45] M. Veselsky, R. W. Ibbotson, R. Laforest, E. Ramakrishnan, D. J. Rowland, A. Ruangma, E. M. Winchester, E. Martin, and S. J. Yennello, Isospin dependence of isobaric ratio Y(H-3) / Y(He-3) and its possible statistical interpretation, Phys. Lett. B **497**, 1 (2001).

[46] F. Rami *et al.*, Isospin Tracing: A Probe of Nonequilibrium in Central Heavy-Ion Collisions, Phys. Rev. Lett. **84**, 1120 (2000).

[47] Yu. B. Gurov, L. Yu. Korotkova, S. V. Lapushkin, R. V. Pritula, B. A. Chernyshev, and T. D. Schurenkova, Yields of triton and ^{3}He produced by nuclei in reactions of stopped pion absorption, Bull. Russ. Acad. Sci. Phys. **78**, 1112 (2014).

[48] T. X. Liu, W. G. Lynch, R. H. Showalter, M. B. Tsang, X. D. Liu, W. P. Tan, M. J. v. Goethem, G. Verde, A. Wagner, H. F. Xi, H. S. Xu, M. A. Famiano, R. T. de Souza, V. E. Viola, R. J. Charity, and L. G. Sobotka, Isospin observables from fragment energy spectra, Phys. Rev. C **86**, 024605 (2012).

[49] F. Guan *et al.*, A compact spectrometer for heavy ion experiments in the Fermi energy regime, Nucl. Instrum. Methods Phys. Res. A **1011**, 165592 (2021).

[50] Y.-J. Wang *et al.*, CSHINE for studies of HBT correlation in heavy ion reactions, Nucl. Sci. Tech. **32**, 4 (2021).

[51] Z. Sun, W.-L. Zhan, Z.-Y. Guo, G. Xiao, and J.-X. Li, Ribll, the radioactive ion beam line in Lanzhou, Nucl. Instrum. Methods Phys. Res. A **503**, 496 (2003).

[52] J. W. Xia, W. L. Zhan, B. W. Wei, Y. J. Yuan, M. T. Song, W. Z. Zhang, X. D. Yang, P. Yuan, D. Q. Gao, H. W. Zhao, X. T. Yang, G. Q. Xiao, K. T. Man, J. R. Dang, X. H. Cai, Y. F. Wang, J. Y. Tang, W. M. Qiao, Y. N. Rao, Y. He *et al.*, The heavy ion cooler-storage-ring project (HIRFL-CSR) at Lanzhou, Nucl. Instrum. Methods Phys. Res. A **488**, 11 (2002).

[53] F. Guan *et al.*, Track recognition for the $\Delta E-E$ telescopes with silicon strip detectors, Nucl. Instrum. Methods Phys. Res. A **1029**, 166461 (2022).

[54] Zhi Yong He, Gen Ming Jin, Zu Yu Li, Li Min Duan, Guang Xi Dai, Bao Guo Zhang, He Yu Wu, Wan Xin Wen, Yu Jin Qi, and Qing Zheng Luo, Emission time scales for light charged particles from symmetric and asymmetric fission processes for Ar-40 + Au-197 reactions at 25 MeV/nucleon, Phys. Rev. C **57**, 1824 (1998).

[55] H. J. Rose and G. A. Jones, A new kind of natural radioactivity, Nature (London) **307**, 245 (1984).

[56] D. N. Poenaru, Y. Nagame, R. A. Gherghescu, and W. Greiner, Systematics of cluster decay modes, Phys. Rev. C **65**, 054308 (2002); **66**, 049902(E) (2002).

[57] M. Warda, A. Zdeb, and L. M. Robledo, Cluster radioactivity in superheavy nuclei, Phys. Rev. C **98**, 041602(R) (2018).

[58] National Nuclear Data Center, Fission data, https://www.nndc.bnl.gov/nudat3/.

[59] Y. Zhang, N. Wang, Q.-F. Li, Li Ou, J.-L. Tian, M. Liu, Kai Zhao, X.-Z. Wu, and Z.-X. Li, Progress of quantum molecular dynamics model and its applications in heavy ion collisions, Front. Phys. (Beijing) **15**, 54301 (2020).

[60] R. J. Charity *et al.*, Systematics of complex fragment emission in niobium-induced reactions, Nucl. Phys. A **483**, 371 (1988).

[61] R. J. Charity *et al.*, Emission of unstable clusters from hot Yb compound nuclei, Phys. Rev. C **63**, 024611 (2001).

[62] J. Aichelin *et al.*, QMD versus BUU/VUU. Same results from different theories, Phys. Lett. B **224**, 34 (1989).

[63] J. Aichelin, "Quantum" molecular dynamics–A dynamical microscopic n-body approach to investigate fragment formation and the nuclear equation of state in heavy ion collisions, Phys. Rep. **202**, 233 (1991).

[64] L.-W. Chen, C. M. Ko, B.-A. Li, and J. Xu, Density slope of the nuclear symmetry energy from the neutron skin thickness of heavy nuclei, Phys. Rev. C **82**, 024321 (2010).

[65] Y. Zhang, Z. Li, C. Zhou, and M. B. Tsang, Effect of isospin-dependent cluster recognition on the observables in heavy ion collisions, Phys. Rev. C **85**, 051602(R) (2012).